Published in final edited form as:
J Neurosci Methods. 2007 March 30; 161(1): 142–154.

Spatial Resolution of EEG Cortical Source Imaging Revealed by Localization of Retinotopic Organization in Human Primary Visual Cortex

Chang-Hwan Im[1], **Arvind Gururajan**[1], **Nanyin Zhang**[2], **Wei Chen**[2], and **Bin He**[1,*]
1 *Department of Biomedical Engineering, University of Minnesota*

2 *Center for Magnetic Resonance Research, Department of Radiology, University of Minnesota*

Abstract

The aim of the present study is to investigate the spatial resolution of electroencephalography (EEG) cortical source imaging by localizing the retinotopic organization in the human primary visual cortex (V1). Retinotopic characteristics in V1 obtained from functional magnetic resonance imaging (fMRI) study were used as reference to assess the spatial resolution of EEG since fMRI can discriminate small changes in activation in visual field. It is well-known that the activation of the early C1 component in the visual evoked potential (VEP) elicited by pattern onset stimuli coincides well with the activation in the striate cortex localized by fMRI. In the present experiments, we moved small circular checkerboard stimuli along horizontal meridian and compared the activations localized by EEG cortical source imaging with those from fMRI. Both fMRI and EEG cortical source imaging identified spatially correlated activity within V1 in each subject studied. The mean location error, between the fMRI-determined activation centers in V1 and the EEG source imaging activation peak estimated at equivalent C1 components (peak latency: 74.8 ± 10.6 ms), was 7 mm (25% and 75% percentiles are 6.45 mm and 8.4 mm, respectively), which is less than the change in fMRI activation map by a 3° visual field change (7.8 mm). Moreover, the source estimates at the earliest major VEP component showed statistically good correlation with those obtained by fMRI. The present results suggest that the spatial resolution of the EEG cortical source imaging is can correctly discriminate cortical activation changes in V1 corresponding to less than 3° visual field changes.

Keywords

EEG; fMRI; Primary visual cortex (striate cortex or V1); Visual Evoked Potential; Retinotopic organization; Cortical source imaging

Introduction

It has been widely accepted that spatial resolution of scalp electroencephalogram (EEG) can be substantially improved by performing source imaging, or solving the inverse problem of EEG (Nunez & Srinivasan, 2005). The spatial resolution of EEG via imaging relies upon many factors such as the number of sensors, number of active sources, source localization algorithms, forward models, noise levels, and so on. Due to the noninvasive nature of EEG it is difficult to establish the spatial resolution through human *in-vivo* experiments; however, the spatial resolution of EEG source imaging can be indirectly estimated by investigating the source localization accuracy. To assess the source localization accuracy various strategies have been

*__Corresponding author:__ Bin He, Ph.D., Department of Biomedical Engineering, University of Minnesota, 7-105 Hasselmo Hall, 312 Church St. S.E., Minneapolis, MN 55455, USA. Tel.: +1-612-626-1115 Fax.: +1-612-626-6583 E-mail: binhe@umn.edu.

used, including: 1) head phantom or animal experimentation (He et al., 1987; Greenblatt and Robinson 1994; Leahy et al., 1998; Baillet et al., 2001), 2) realistic simulations assuming few dipolar sources or cortical patches (He et al., 2002a,b; Darvas et al., 2004; Hori et al., 2004; Ding et al., 2005; Im et al., 2005a), 3) use of well-known sensory related anatomical landmarks (Darvas et al., 2005; Yao and Dewald, 2005), and 4) comparison with invasive measurements (Lantz et al., 2001; He et al., 2002c; Zhang et al., 2003; Zhang et al., 2006). The first two strategies are straightforward because the true source locations are given, but they may not fully reflect complex conditions in *in-vivo* human experiments. On the contrary, the latter two strategies are applicable only for some restricted cortical areas and hard to be applied to normal human subjects.

Comparing EEG sources with functional magnetic resonance imaging (fMRI) activation can be a means to estimate the EEG (or MEG) source localization accuracy. Since fMRI are capable of producing spatial resolutions as high as 1–3 mm, the fMRI activation map may be used as a reference. Although there are some intrinsic discrepancies between fMRI and EEG (or MEG) due to the fundamental difference of hemodynamic and electrophysiological processes (Nunez and Silberstein 2000; Bonmassar et al., 2001; Disbrow et al., 2005), the comparison between fMRI activations and EEG (or MEG) sources has been regarded as a useful measure, particularly in simple sensory tasks (Stippich et al., 1998; Vitacco et al., 2002; Moradi et al., 2003).

While the source localization accuracy of EEG/MEG has been previously studied with respect to a stationary stimulus, little is known about the source localization accuracy of EEG corresponding to the change in sensory stimulation. The definition of spatial resolution should include not only how large the mean localization error is, but also how well a method can detect small changes or spatial movement of the activations, that is, the sensitivity of the method. Suppose that there are three temporally uncorrelated sources along a certain line and the locations are spaced with an inter-source distance of 5 mm. For this case, each source location can be estimated independently at three different time windows. There may be two different localization results: one possible case is that the three estimated sources are localized at the central source; while the other case is that the three estimated sources are biased from the actual source locations toward a certain direction with a consistent localization error of 3.33 mm. If we only examine the mean localization error, the two cases would look identical. However, the first case cannot discriminate the 10 mm change of source location, but the second case can reflect the source changes while preserving consistent distance from the actual sources. Thus, the spatial resolution of the second case is better than that of the first case. The present study was aimed to realize this kind of paradigm in human *in-vivo* experiments and investigate the spatial resolution of EEG cortical source imaging by comparing with that of fMRI.

In human *in-vivo* studies, such a ‘moving activation’ model can be simulated using various tasks, e.g. motor/sensory-related tasks (Darvas et al., 2004) and tonotopic organization of human auditory cortex (Talavage et al., 2004). In particular, the retinotopic activity in the human visual cortex (Sereno et al., 1995; DeYoe et al., 1996; Engel et al., 1997; Warnking et al., 2002; Grill-Spector and Malach 2004) has been well studied. The retinotopic maps constructed using fMRI have been frequently applied to visual ERP studies in order to identify functional or anatomical locations of the localized ERP sources (Vanni and Warnking et al., 2004; Vanni and Dojat et al., 2004; Di Russo et al., 2005). It is a well-known phenomenon that the neuronal sources related to the early VEP components in response to the pattern-onset/reversal visual stimulation correspond well to the activations in the human primary visual cortex (striate cortex or V1) acquired from fMRI (Di Russo et al., 2001; Vanni and Warnking et al., 2004). Many studies have been performed to reveal the discrepancy between the fMRI loci at V1 and EEG or MEG source locations estimated from either dipole models (Gratoon et

al., 1997; Roberts et al., 2000) or distributed source models (Moradi et al., 2003), and a large variation ranging from 5 mm to several cm has been observed in the previous studies.

To the best of our knowledge, a systematic comparison of the V1 source locations estimated from fMRI and EEG corresponding to different visual stimuli with varied visual fields has not been reported. In the present study, we varied the location of a small circular checkerboard stimulus along the horizontal meridian, expecting the gradual movement of the corresponding activations along the calcarine fissure from posterior to anterior part of V1. The foci of the cortically constrained distributed sources (or cortical sources) estimated from 128-channel dense array EEG measurements were then compared with the V1 activation centers identified by fMRI, to investigate if the spatial resolution of EEG cortical source imaging is high enough to discriminate the small activation changes in V1.

Materials and Methods

Human Subjects

Ten paid volunteer subjects (2 females and 8 males, mean age 22.0, range 19–30 years) participated in the visual evoked potential (VEP) recordings as well as the structural MRI (sMRI) and fMRI study. All subjects gave their informed consent before the study. Data sets from seven subjects (2 females and 5 males, mean age 21.6, range 20–24 years) that showed typical VEP signals with fewer artifacts were selected for the analysis. Three subjects did not concentrate on the experimentation and thus their data contained a lot of eye blink artifacts or contaminations by voluntary movements. The data from these three subjects were excluded from the analysis.

Stimuli

The stimuli were generated with STIM^2 software (Compumedics, Inc., El Paso, TX). The VEP experiments were performed in the Biomedical Functional Imaging and Neuroengineering Laboratory (University of Minnesota, MN) where stimuli were generated with a DLP videoprojector (Epson PowerLite 74c, Epson Inc., Japan) and displayed on a white screen. The structure and functional MRI (s/fMRI) studies were performed in the Center for Magnetic Resonance Research (University of Minnesota, MN). The stimuli there were also generated with a DLP videoprojector (SANYO PRO xTrax, Sanyo Inc., Japan) and projected onto a back projection screen which the subjects viewed via a mirror. The visual angles, contrast, and timing parameters of the visual stimuli were the same for both the fMRI and VEP experiments. Figure 1 displays the stimuli used for the present study. The stimuli consisted of circular black-white checkerboards; each stimulus had a diameter of 4.8° visual angle and a spatial modulation of 1.5 cycles per degree. An ‘X’-shape cross-mark, of which the color and visual angle were red and 1° respectively, was used for the central fixation point. The stimuli were placed on the horizontal meridian with three different visual angles: 3° (range 0.6° – 5.4°), 6° (range 3.6° – 8.4°), and 9° (range 6.6° – 11.4°) measured from the central fixation point to the center of each stimulus. The stimuli were named L3, L6, L9, R3, R6, and R9 (L: left visual field; R: right visual field; numbers: visual angles), as shown in Figure 1. To meet the targeted visual angles, the size of the circle and distance between the circle and the fixation point was manually measured and adjusted in each experiment. Both the fMRI and VEP experiments were divided into three sessions according to the different visual angles (3°, 6°, and 9°). The size and visual angles of the visual stimuli were determined empirically after several test experiments. Subjects were trained to focus on the central fixation point and instructed to be relaxed and not to blink their eyes too frequently. Each stimulus was flashed for 250 ms with an inter-stimulus interval (only fixation point) of 250 ms. Left and right stimuli were presented in two task blocks, which lasted for 20 s. Two task blocks were separated by a 40 s control or resting block, when only the fixation point was presented.

VEP Recording and Data Processing

The VEP was recorded with two SynAmps^2 amplifiers (Compumedics, Inc., El Paso, TX) connected with a 128-channel electrode cap (QuickCap, Compumedics, Inc., El Paso, TX), for which the electrodes were evenly distributed according to the extended 10–20 system. The ground electrode for the 128-channel cap was located at a midline frontal location halfway between the 10/20 positions of FPz and Fz with the reference electrode location halfway between the 10/20 positions of CPz and Cz. The VEP signals were extracted from continuously acquired EEG data, low-pass filtered at 30 Hz (12 dB/octave), and sampled at 100 Hz. In the first stage of offline analysis noisy periods, visible eye blinks and artifacts related to eye movements were rejected either automatically or manually within the Neuroscan SCAN software package (Compumedics, Inc., El Paso, TX). After segmentation into single sweep epochs beginning 50 ms before the stimulus onset and ending 300 ms after the stimulus onset, a constant baseline correction was performed for each segment. Bad channels of which the signal included unexpected fluctuation or distortion was rejected manually by tracking each channel signal. After the averaging process, we checked if the VEP waveforms and topographic maps showed typical trends of VEPs. If they were not, we repeated the protocol again or discarded the subject's data. The physical landmarks (nasion and two auricular points) and electrode positions were digitized using a Polhemus Fastrak digitizer (Polhemus, Colchester, VT) and 3D SpaceDx software contained within the SCAN software package.

MRI Scanning and Analysis

Both sMRI and fMRI data were collected using a 3T MRI system (Siemens Trio, Siemens, Erlangen, Germany). Multiple-slice T_1-weighted MR images (matrix size 256 × 256 × 256, field of view 256 × 256 × 256 mm^3) were acquired using a Turboflash sequence (TR/TE=20 ms/5 ms) (Hasse 1990). The T_2*-weighted fMRI data were acquired from ten axial slices (matrix size 64 × 64, 5mm thickness) covering the calcarine fissure using an echo planar imaging (EPI) sequence (TR/TE=1000 ms/35 ms). The data analysis was performed using the software package STIMULATE (Strupp 1996). The fMRI images for each stimulation condition were analyzed using the period cross-correlation method (Bandettini et al., 1992), in which the cross-correlation coefficient (CC) between the signal time course and a reference function was calculated for each pixel.

Surface models of each subject's cortex were constructed from tracings of the gray/white matter boundary in T_1-weighted images, which is relatively easier to be detected than the other borders. The traced contours were combined into a tessellated surface including about 800,000 triangular elements and 400,000 vertices by using BrainSuite, a software package developed at the University of Southern California (Shattuck and Leahy 2002). For each pixel in the fMRI images, the CC value was assigned to the single nearest point on the reconstructed surface. It was also assigned to neighboring points within a radius proportional to half the size of an imaging voxel (DeYoe et al., 1996; Engel et al., 1997). The complete pattern was then slightly smoothed by an average of the activity at each node and its neighbors (DeYoe et al., 1996).

EEG Cortical Source Imaging

In the present study, a realistic geometry head model was considered for accurate EEG forward calculation (He et al., 1987; Hämäläinen and Sarvas, 1989). A first order node-based boundary element method (BEM) was used to construct a lead field matrix which relates sources to the potential at the scalp electrodes. In the present study three-layer tessellated boundary surfaces, consisting of the inner and outer skull boundary and scalp surface, were generated using CURRY5 for windows (Compumedics, Inc., El Paso, TX). About 7,000 boundary elements and 3,500 surface nodes were generated from each subject's T_1-weighted MR images. The relative conductivity values of the brain, skull, and scalp were assumed to be 1, 1/16, and 1, respectively (Haueisen et al., 1997; Oostendorp et al., 2000). The electrode locations were

fitted to the boundary elements using anatomical landmarks (nasion and two auricular points) (de Munck et al., 1991) and adjusted manually in the CURRY5 software platform.

Since synchronously activated pyramidal cortical neurons, which are located perpendicularly on the cortical surface, are widely believed to be the main EEG and MEG generators, many recent studies have adopted this physiological phenomenon as a basic anatomical constraint in EEG or MEG source imaging (Dale and Sereno, 1993; Kincses et al., 1999; Dale et al., 2000; Babiloni et al., 2003, 2005). The source imaging with the anatomical constraint, which has been often called cortically distributed source modeling or cortical source imaging, resulted in the elimination of spurious sources (Baillet et al., 1998) as well as the reduction of crosstalk distribution (Liu et al., 1998), compared to conventional volume based imaging techniques.

To impose the anatomical constraint, many dipolar sources were placed on the same cortical surface which had been used for the fMRI surface mapping. Although developments of medical image processing and high resolution sMRI enabled us to get a high resolution cortical surface with sub-millimeter modeling errors (Dale et al., 1999; Fischl and Dale 2000), it is computationally inefficient to use whole cortical surface vertices for the source reconstruction purpose because of the increased underdetermined relationship between limited numbers of sensors and larger numbers of source locations. To reduce the number of possible source locations, a smaller number of vertices was downsampled from the cortical surface as regularly as possible and used for source reconstruction purpose; whereas the original mesh information was used only for visualization purpose (Dhond et al., 2003; Lin et al., 2004). In the present study, about 15,000 vertices were downsampled from more than 400,000 original cortical vertices. The orientations of the cortical sources were not constrained because very accurate anatomical structure around the calcarine fissure could not be obtained in some subjects due to spatial inhomogeneity in the MRI T_1-weighted images (e.g. see Fig. 4 in advance).

To reconstruct the cortically distributed brain sources, we used a linear estimation approach (Dale and Sereno 1993; Dale et al., 2000). The expression for the inverse operator **W** is

$$\boldsymbol{W} = \boldsymbol{RA}^{\mathrm{T}}(\boldsymbol{ARA}^{\mathrm{T}} + \lambda^2 \boldsymbol{C})^{-1}, \quad (1)$$

where $\boldsymbol{A}$ is the lead field matrix, $\boldsymbol{R}$ is a source covariance matrix, and $\boldsymbol{C}$ is a noise covariance matrix. The source distribution can be estimated by multiplying the measured signal at a specific instant x by $\boldsymbol{W}$. If we assume that both $\boldsymbol{R}$ and $\boldsymbol{C}$ are scalar multiples of identity matrix, this approach becomes identical to minimum norm estimation (Liu et al., 2002). In the present study, the source covariance matrix $\boldsymbol{R}$ was assumed to be a diagonal matrix, which means that we ignored relationships between neighboring sources. The lead field weightings (Lin et al., 2004, 2006) were imposed to each diagonal entry of $\boldsymbol{R}$. In the present study, a pre-stimulus time window was used to calculate $\boldsymbol{C}$. λ^2 is a regularization parameter and was determined systematically using the L-curve method (Hansen 1991). The EEG inverse problem can also be nicely solved with less phantom or noisy sources if we can restrict the possible source locations to more probable brain regions based on some functional *a priori* information. Since we already identified from previous studies and our fMRI studies that the EEG sources related to the early visual process would appear around the visual cortex, we gave the source points located around occipital lobe a higher probability to be estimated in the EEG inverse. We imposed the probability to the EEG inverse solution by giving different weighting values to the diagonal terms of $\boldsymbol{R}$. If a source belonged to the predetermined regions, 1 was multiplied by its corresponding diagonal term; otherwise, 0.1 was multiplied (Liu et al., 1998, Im et al., 2005b). The area where the functional constraints were imposed was large enough to cover the entire human visual cortex (e.g. see Figure 2a), to ensure that the functional *a priori* information does not directly affect the solution accuracy.

Determination of C1 Peak Latency and Visualization of fMRI Images

In the typical experiments that used upper or lower visual fields, the early VEP component called C1 could be easily detected around parieto-occipital electrodes (e.g. PO3, POz, PO4, etc.) because the source orientation is approximately inferior-to-superior (upper visual field) or superior-to-inferior (lower visual field) direction, which makes strong positive or negative potential around the top of the electrode cap (Di Russo et al., 2001; Vanni and Warnking et al., 2004). In the present experiment, however, the left-to-right or right-to-left directional component was expected to be dominant in the source orientation vector because the actual source will reside inside the fundus of the calcarine fissure. Therefore, we relied upon the topographic map to search for the timing which is equivalent to the C1 component observed in the upper or lower visual field experiments. Figure 2 shows two examples of the potential topographic maps and waveforms at some electrodes, which are located around the maximum of the scalp potential map. Figures 2(a), (b) and 2(c), (d) are the topographic maps and waveforms of protocols L9 and R3, respectively. The equivalent C1 peaks of L9 and R3 were estimated as 73 ms and 59 ms, respectively. It is anticipated from the topographic maps that a deeper source of which the position was biased toward the anterior V1 would be estimated for L9 and a shallow source located around the posterior visual cortex would be estimated for R3. Moreover, it is also anticipated that a single dipolar source pattern would be reconstructed if EEG source imaging is applied to the topographic map.

The latencies of the equivalent C1 peaks were diverse in the individual subjects, but the mean value of all 42 data sets was 74.8 ± 10.6 ms, which was close to the C1 peak latencies reported in previous literatures (Di Russo et al., 2001; Vanni and Warnking et al., 2004).

For the fMRI results, strong and clear activations were observed around the calcarine fissure of the contralateral V1 in most subjects. In some subjects, a small activation was also observed in the extrastriate cortex, but it was never seen in the ipsilateral V1. To leave only the V1 activations, we first cut out the relatively small activations below a threshold value of 0.9 × maximum CC, which was determined empirically after visual inspection of all activation images. The maximum CC values of each fMRI data set were ranged from 0.71 to 0.89.

Results

EEG Cortical Source Imaging and fMRI Results

Figures 3 and 4 show examples of the EEG cortical source estimates and the corresponding fMRI activation maps for subjects 1 and 7, respectively. We applied a consistent threshold (0.25 in normalized EEG source power) to cut out small activations in the EEG cortical source estimates. Although the typical anatomical structures of the calcarine fissure could not be very accurately represented by the cortical surface segmentation in some subjects (e.g. see subject 7), the fMRI activations of both subjects showed clear movement from the posterior to the anterior part of V1, which coincides well with previous fMRI findings (Engel et al., 1997; Sereno et al., 1995; Grill-Spector and Malach 2004). Moreover, it was seen from visual inspection of the distributions that the changes of the fMRI and EEG sources are correlated with each other.

Comparison of Location Difference

We first calculated the distance between the fMRI activations and EEG source estimates. For fMRI, we used the center of gravity of the V1 activation (Moradi et al., 2003; Di Russo et al., 2001) which exceeded the same threshold value used for the visualization. For EEG, however, the center of gravity of the activation was much more sensitive to the threshold value than the fMRI. Thus, we picked the peak value of the activation, which has been used as a typical

measure in EEG/MEG distributed source analysis studies (Pascual-Marqui 2002; Lin et al., 2006).

Figures 5 and 6 illustrate the centers of fMRI activations and peak positions of EEG source distributions co-registered in the anatomical structures of subject 1 and 7, respectively, where we can compare the spatial locations of the activations acquired from the two modalities more clearly. We summarized the location differences evaluated for all seven subjects in Table I. The median of location errors between fMRI centers and EEG source peaks was 7 mm (25% and 75% percentiles are 6.45 mm and 8.4 mm, respectively). For comparison, the average distance moved by the fMRI centers with respect to a 3° (from 3° to 6°) and a 6° (from 3° to 9°) visual field change is also presented in the table. It can be seen from the table that the location difference between the two modalities (7 mm) is smaller than the fMRI activation changes corresponding to 3° visual field changes (7.8 mm). When nonlinear interpolation was applied, the 7 mm location difference corresponded to a 2.7° visual field change observed in fMRI, which is slightly larger than half the size of the stimuli (2.4°) and less than the visual angle distance between two neighboring circles (3°) in the present experiment.

Comparison of Moving Patterns

Considering the previous literatures on the location errors between fMRI and EEG sources (Stippich et al., 1999; Vitacco et al., 2002; Moradi et al., 2003), a 7 mm error for a 128-channel EEG system looks like a reasonable value. Considering the small activation changes in fMRI (less than 10 mm), however, the location error could be around 7 mm when the EEG source locations are not correlated with fMRI activations. Although we observed from the two examples (subjects 1 and 7) presented in Figures 3~6 that the EEG sources moved from the posterior to the anterior V1 in correspondence to the visual field change, we tried to measure quantitatively whether the EEG source location changes are actually correlated with the visual field changes or are just random changes within the error bound of about 7 mm.

First, we calculated the moving distance of the EEG source peaks with respect to the visual field changes in order to show that the EEG source locations are actually changing. Table I presents the moving distance of both the fMRI centers and EEG source peaks with respect to the 3° and 6° visual field changes. To assess whether the EEG sources are stationary, we performed non-parametric statistical analysis. We calculated a probability of equality between a stationary case (all the values are zero) and our results, using Wilcoxon rank sum test which is embedded in Matlab statistics toolbox (Mathworks, Inc., Natick, US). The probability for the EEG sources to be stationary was as low as $p = 0.0006$, which demonstrates that the EEG sources are not stationary, but are sensitive to the visual field changes. To assess whether the average moving distances depend on the technique used, we performed paired statistic test. Considering the small number of samples, we used Wilcoxon rank sum test for equal medians, which is a kind of nonparametric statistical analysis techniques. The average moving distances showed correlation ($p = 0.1713$ for 3° movement and $p = 0.3176$ for 6° movement) to some extent, but we could not confirm that the two techniques are correlated yet because we did not check the moving directions.

We then compared the moving patterns of the fMRI centers and EEG source peaks to confirm the movements of the fMRI and EEG activations are correlated with each other. Table II compares the volume angles between two vectors connecting first (3° visual field) and second (6° visual field) activations and second (6° visual field) and third (9° visual field) activations. The angle exceeding 90° represents negative movement, i.e. the activations do not move forward. The values ranged from 1.2° to 89.1° in either fMRI or EEG. The median values of fMRI were 50.7° and 32.5° for left and right stimulus, respectively. The median values of EEG were 59.8° and 51.3° for left and right stimulus, respectively. The results demonstrate that the fMRI and EEG sources moved forward to a certain direction.

We then further compared the mean moving directions of the fMRI centers and EEG source peaks to confirm that both activations moved in similar directions. The mean moving direction was defined as a vector which starts from the first activation location (3° visual field) and passes through the middle of second (6° visual field) and third (9° visual field) activations. In Figures 5 and 6, the examples of the mean moving directions are illustrated with red dashed lines and blue dash-dot lines. Table III shows the angular difference between the mean moving directions of fMRI and EEG activations. Inspiringly, the median of differences was as low as 20° and 10.1° for left and right stimuli, respectively. We also performed a non-parametric statistical analysis to show that the moving directions are correlated. The analysis was performed separately for the two different conditions, left and right stimulus. We compared equality between 100 uniformly distributed random numbers generated on [0°, 180°], which simulate randomly moving activations, and the differences of moving directions between fMRI and EEG activations, using Wilcoxon rank sum test for equal medians. For left stimulus, the probability of equality was as low as $p = 0.00009$; for right stimulus, the probability was as low as $p = 0.0004$. The statistical analysis results demonstrate that the moving directions between fMRI and EEG activations are highly correlated.

Discussion and Conclusions

Previous studies have used a stationary stimulus and found strong spatial correlation between the fMRI activations in V1 and the neuronal activities at early VEP component. Such a stationary stimulus, however, could not fully justify that the EEG can detect the small changes of brain activations in V1. In the present study, the quantitative comparison study demonstrated that both fMRI and EEG activations moved forward to a certain direction corresponding to the visual field changes and the moving directions were strongly correlated with each other. The present statistical analysis demonstrates that the average location error of 7 mm originated neither from a stationary source nor from randomly moving activations. The strongly correlated moving patterns between fMRI and EEG activations can be an evidence to show that the EEG cortical source imaging can detect at least 3° visual field changes.

There can be several sources of the location error between fMRI and EEG imaging results in the present study. Inaccurate cortical surface segmentation can be a possible source of the location error. Some subjects' sMRI data were not very homogeneous because of the field inhomogeneity inside the high-field (3T) MRI magnet, resulting in slightly unclear anatomical structures around V1. Since we restricted the possible source locations only to the tessellated cortical surface, the actual source location may not be included in the inaccurate cortical surface model. Then, the inverse process would find the currently best source location where the crosstalk with the actual source location (Liu et al., 1998) is largest.

More accurate and realistic forward calculations are expected to increase the source localization accuracy of EEG. The influence of the tissue (skull and/or white matter) anisotropy to the EEG inverse problems has not been well investigated in *in-vivo* experimental studies, but some simulation or phantom experiment studies (Baillet et al., 2001; Wolters et al., 2006) showed that the tissue anisotropy can affect the inverse solution accuracy to some extent, particularly in estimating deep neocortical sources. Therefore, it is possible that the anisotropy of the skull and white matter might contribute to the localization error.

Although the protocol used in the present study can generate highly reproducible activations (as shown previously -- e.g. See Figure 9 in (Di Russo et al. 2001)), separate acquisition of fMRI and VEP data can also contribute to the location errors between the two modalities. Recent studies have shown that the mean standard deviation of EEG or MEG source locations for a very simple auditory or somatosensory stimulus could reach to 5 mm, when the same protocol was repeated to the same subjects (Kwon et al., 2002; Schaefer et al., 2002). Moreover,

different environments in the fMRI and VEP recordings such as slight differences in the contrast and brightness of the visual stimuli may cause some discrepancies between the two results. Therefore, it is desirable to acquire the fMRI and EEG data in a single session to avoid possible discrepancies due to the different environmental and cognitive states in separate examinations. However, simultaneous recording of fMRI and EEG is challenging since the EEG recordings are prone to large artifacts induced by the high-frequency gradient and RF pulses inside the MR scanner, namely pulse sequence artifact (PSA), and motion of EEG leads within the static magnetic field, such as ballistocardiogram artifact (BA) caused by the pulsatile motion related to heart beat (Allen et al., 2000). Since recent progresses of MR-compatible EEG recording systems and signal processing techniques have enabled us to get consistent EEG signals during fMRI scanning inside an MRI scanner (Comi et al., 2005; Becker et al., 2005), it is expected that the simultaneous fMRI-EEG recording would become a promising tool to reduce the discrepancy between the two modalities in the near future.

Many previous studies have used the dipole model to localize the early VEP activity in the V1 (Di Russo, et al., 2001; 2005; Vanni and Warnking et al., 2004). Since the scalp potential topography at early latencies shows dipolar field patterns, the use of the single dipole model could represent the V1 activation fairly well. On the other hand, localization of the V1 activity using a cortically distributed source model is difficult because superficial cortical sources may prevent the deeper sources from being estimated. Since these kinds of source localization problems have always been a challenging problem in the EEG or MEG source inverse, comparison of localized retinotopic activities can be a useful means to study the source localization accuracy of EEG or MEG inverse algorithms.

In summary, the present study demonstrated that the activations in the V1 found by fMRI and the EEG cortical source imaging at early VEP component are well correlated with each other and the spatial resolution of EEG cortical source is high enough to discriminate the small cortical activation changes in V1 corresponding to 3° visual field changes. The present study can not only demonstrate the accuracy and reliability of EEG source localization data, but also provide neuroscience researchers with a guideline to design paradigms which aim to get high resolution images. The locations of neuronal sources related to the earliest major visual activity have been revealed to be located in V1, but those at later latencies of VEP signals are still a controversial issue (Di Russo et al., 2005). In the present study, we focused only on the localization accuracy and spatial resolution of the EEG cortical source imaging in V1, but it is anticipated that the EEG source imaging would be useful in revealing the visual processes in the human visual cortex during more elaborate scenarios.

Acknowledgements

We thank John Swain, Cameron Sheikholeslami, and Varun Garg for assistance in VEP experimentation, and the anonymous reviewers for constructive comments to the original version of the manuscript. This work was supported in part by NSF BES-0411898, NIH RO1 EB00178, NIH RO1 EB00239, the Biomedical Engineering Institute of the University of Minnesota, BTRR P41 008079, KECK Foundation and MIND Institute. CH Im was supported in part by a Korea Research Foundation Fellowship funded by the Korean Government (MOEHRD) (M01-2005-000-10132-0).

References

Allen PJ, Josephs O, Turner R. A method for removing imaging artifact from continuous EEG recorded during functional MRI. Neuroimage 2000;12:230–239. [PubMed: 10913328]

Babiloni F, Babiloni C, Carducci F, Romani GL, Rossini PM, Angelone LM, Cincotti F. Multimodal integration of high-resolution EEG and functional magnetic resonance imaging data: a simulation study. Neuroimage 2003;19:1–15. [PubMed: 12781723]

Babiloni F, Babiloni C, Carducci F, Cincotti F, Astolfi L, Basilisco A, Rossini PM, Ding L, Ni Y, Cheng J, Christine K, Sweeney J, He B. Assessing time-varying cortical functional connectivity with the

multimodal integration of high resolution EEG and fMRI data by Directed Transfer Function. Neuroimage 2005;24(1):118–131. [PubMed: 15588603]

Baillet, S. Toward Functional Brain Imaging of Cortical Electrophysiology Markovian Models for Magneto and Electroencephalogram Source Estimation and Experimental Assessments. University of Paris XI; 1998. Ph. D. dissertation

Baillet S, Riera JJ, Marin G, Mangin JF, Aubert J, Garnero L. Evaluation of inverse methods and head models for EEG source localization using a human skull phantom. Phys Med Biol 2001;46:77–96. [PubMed: 11197680]

Bandettini PA, Wong EC, Hinks RS, Tikofsky RS, Hyde JS. Time course EPI of human brain function during task activation. Magn Reson Med 1992;25:390–397. [PubMed: 1614324]

Becker R, Ritter P, Moosmann M, Villringer A. Visual Evoked Potentials Recovered From fMRI Scan Periods. Hum Brain Mapp 2005;26:221–230. [PubMed: 15954138]

Bonmassar G, Schwartz DP, Liu AK, Kwong KK, Dale AM, Belliveau JW. Spatiotemporal brain imaging of visual-evoked activity using interleaved EEG and fMRI recordings. Neuroimage 2001;13:1035–1043. [PubMed: 11352609]

Comi E, Annovazzi P, Silva AM, Cursi M, Blasi V, Cadioli M, Inuggi A, Falini A, Comi G, Leocani L. Visual evoked potentials may be recorded simultaneously with fMRI scanning: A validation study. Hum Brain Mapp 2005;24:291–298. [PubMed: 15678479]

Dale AM, Sereno M. Improved localization of cortical activity by combining EEG and MEG with MRI surface reconstruction: a linear approach. J Cognit Neurosci 1993;5:162–176.

Dale AM, Fischl B, Sereno MI. Cortical Surface-Based Analysis I. Segmentation and Surface Reconstruction Neuroimage 1999;9:179–194.

Dale AM, Liu AK, Fischl BR, Buckner RL, Belliveau JW, Lewine JD, Halgren E. Dynamic Statistical Parametric Mapping: Combining fMRI and MEG for High-Resolution Imaging of Cortical Activity. Neuron 2000;26:55–67. [PubMed: 10798392]

Darvas F, Pantazis D, Kucukaltun-Yildirim E, Leahy RM. Mapping human brain function with MEG and EEG: methods and validation. Neuroimage 2004;23:S289–S299. [PubMed: 15501098]

Darvas F, Rautiainen M, Pantazis D, Baillet S, Benali H, Mosher JC, Garnero L, Leahy RM. Investigations of dipole localization accuracy in MEG using the bootstrap. Neuroimage 2005;25(2):355–368. [PubMed: 15784414]

de Munck JC, Vijn PCM, Spekrijse HA. A Practical method for determining electrode positions on the head. Electroenceph Clin Neurophys 1991;79:85–87.

DeYoe EA, Carman GJ, Bandettini P, Glickman S, Wieser J, Cox R, Miller D, Neitz J. Mapping striate and extrastriate areas in human cerebral cortex. Proc Natl Acad Sci USA 1996;93:2382–2386. [PubMed: 8637882]

Dhond RP, Marinkovic K, Dale AM, Witzel T, Halgren E. Spatiotemporal maps of past-tense verb inflection. Neuroimage 2003;19:91–100. [PubMed: 12781729]

Ding L, Lai Y, He B. Low resolution brain electromagnetic tomography in a realistic geometry head model: a simulation study. Phys Med Biol 2005;50(1):45–56. [PubMed: 15715421]

Di Russo F, Martinez A, Sereno MI, Pitzalis S, Hillyard SA. Cortical Sources of the Early Components of the Visual Evoked Potential. Hum Brain Mapp 2001;15:95–111. [PubMed: 11835601]

Di Russo F, Pitzalis S, Spitoni G, Aprile T, Patria F, Spinelli D, Hillyard SA. Identification of the neural sources of the pattern-reversal VEP. Neuroimage 2005;24:874–886. [PubMed: 15652322]

Disbrow EA, Slutsky DA, Roberts TPL, Krubitzer LA. Functional MRI at 1.5 tesla: A comparison of the blood oxygenation level-dependent signal and electrophysiology. Proc Natl Acad Sci USA 2005;97:9718–9723. [PubMed: 10931954]

Engel SA, Glover GH, Wandell BA. Retinotopic organization in human visual cortex and the spatial precision of functional MRI. Cereb Cortex 1997;7:181–192. [PubMed: 9087826]

Fischl B, Dale AM. Measuring the thickness of the human cerebral cortex from magnetic resonance images. Proc Natl Acad Sci USA 2000;97:11050–11055. [PubMed: 10984517]

Gratton G, Fabiani M, Corballis PM, Hood DC, Goodman-Wood MR, Hirsch J, Kim K, Friedman D, Gratoon E. Fast and localized event-related optical signals (EROS) in the human occipital cortex: comparisons with the visual evoked potential and fMRI. Neuroimage 1997;6:168–180. [PubMed: 9344821]

Greenblatt R, Robinson S. A simple head shape approximation for the 3 shell model. Brain Topogr 1994;64(4):331.

Grill-Spector K, Malach R. The human visual cortex. Annu Rev Neurosci 2004;27:649–677. [PubMed: 15217346]

Hämäläinen MS, Sarvas J. Realistic conductivity geometry model of the human head for interpretation of neuromagnetic data. IEEE Trans Biomed Eng 1989;36:165–171. [PubMed: 2917762]

Hansen P. Analysis of discrete ill-posed problems by means of the L-curve. SIAM Rev 1992;34:561–80.

Haase A. Snapshot FLASH MRI: Applications to T1, T2, and chemical-shift imaging. Magn Reson Med 1990;13:77–89. [PubMed: 2319937]

Haueisen J, Ramon C, Eiselt M, Brauer H, Nowak H. Influence of tissue resistivities on neuromagnetic fields and electric potentials studied with a finite element model of the head. IEEE Trans Biomed Eng 1997;44:727–735. [PubMed: 9254986]

He B, Musha T, Okamoto Y, Homma S, Nakajima Y, Sato T. Electric dipole tracing in the brain by means of the boundary element method and its accuracy. IEEE Trans Biomed Eng 1987;34:406–414. [PubMed: 3610187]

He B, Yao D, Lian J. High Resolution EEG: On the Cortical Equivalent Dipole Layer Imaging. Clin Neurophysiol 2002a;113:227–235. [PubMed: 11856627]

He B, Yao D, Lian J, Wu D. An Equivalent Current Source Model and Laplacian Weighted Minimum Norm Current Estimates of Brain Electrical Activity. IEEE Trans Biomed Eng 2002b;49:277–288. [PubMed: 11942719]

He B, Zhang X, Lian J, Sasaki H, Wu D, Towle VL. Boundary element method-based cortical potential imaging of somatosensory evoked potentials using subjects' magnetic resonance images. Neuroimage 2002c;16(3):564–576. [PubMed: 12169243]

Hori J, Aiba M, He B. Spatio-temporal Cortical Source Imaging of Brain Electrical Activity by means of Time-Varying Parametric Projection Filter. IEEE Trans Biomed Eng 2004;51:768–777. [PubMed: 15132503]

Im CH, Jung HK, Fujimaki N. Anatomically constrained dipole adjustment (ANACONDA) for accurate MEG/EEG focal source localizations. Phys Med Biol 2005a;50:4931–4953. [PubMed: 16204881]

Im CH, Jung HK, Fujimaki N. fMRI-constrained MEG source imaging and consideration of fMRI invisible sources. Hum Brain Mapp 2005b;26:110–118. [PubMed: 15858829]

Kincses WE, Braun C, Kaiser S, Elbert T. Modeling extended sources of event-related potentials using anatomical and physiological constraints. Hum Brain Mapp 1999;8:182–193. [PubMed: 10619413]

Kwon H, Lee YH, Kim JM, Park YK, Kuriki S. Localization accuracy of single current dipoles from tangential components of auditory evoked fields. Phys Med Biol 2002;47:4145–4154. [PubMed: 12502039]

Lantz G, Menendez RGD, Andino SG, Michel CM. Noninvasive localization of electromagnetic epileptic activity. II. Demonstration of sublobar accuracy in patients with simultaneous surface and depth recordings. Brain Topogr,a 2001;14(2):139–147.

Leahy RM, Mosher JC, Spencer ME, Huang MX, Lewine JD. A study of dipole localization accuracy for MEG and EEC using a human skull phantom. Electroencephalogr Clin Neurophysiol 1998;107 (2):159–173. [PubMed: 9751287]

Lin F-H, Witzel T, Hämäläinen MS, Dale AM, Belliveau JW, Stufflebeam SM. Spectral spatiotemporal imaging of cortical oscillations and integrations in the human brain. Neuroimage 2004;23:582–595. [PubMed: 15488408]

Lin F-H, Witzel T, Ahlfors SP, Stufflebeam SM, Belliveau JW, Hämäläinen MS. Assessing and improving the spatial accuracy in MEG source localization by depth-weighted minimum-norm estimates. Neuroimage 2006;31:160–171. [PubMed: 16520063]

Lin F-S, Belliveau JW, Dale AM, Hämäläinen MS. Distributed current estimates using cortical orientation constraints. Hum Brain Mapp 2006;27:1–13. [PubMed: 16082624]

Liu AK, Belliveau JW, Dale AM. Spatiotemporal imaging of human brain activity using functional MRI constrained magnetoencephalography data: Monte Carlo simulations. Proc Natl Acad Sci USA 1998;95:8945–8950. [PubMed: 9671784]

Liu AK, Dale AM, Belliveau JW. Monte Carlo simulation studies of EEG and MEG localization accuracy. Hum Brain Mapp 2002;16:47–62. [PubMed: 11870926]

Moradi F, Liu LC, Cheng K, Waggoner RA, Tanaka K, Ioannides AA. Consistent and precise localization of brain activity in human primary visual cortex by MEG and fMRI. Neuroimage 2003;18:595–609. [PubMed: 12667837]

Nunez PL, Silberstein RB. On the relationship of synaptic activity to macroscopic measurements: does co-registration of EEG with fMRI make sense? Brain Topogr 2000;13:79–96. [PubMed: 11154104]

Nunez, PL.; Srinivasan, R. Electric Fields of the Brain : The Neurophysics of EEG. 2nd Ed. Oxford University Press;

Oostendorp TF, Delbeke J, Stegeman DF. The conductivity of the human skull: Results of in vivo and in vitro measurements. IEEE Trans Biomed Eng 2000;47:1487–1492. [PubMed: 11077742]

Pascual-Marqui R. Standardized low-resolution brain electromagnetic tomography (sLORETA): technical details. Meth Findings Exp Clin Pharmacol 2002;24:5–12.

Roberts TP, Disbrow EA, Roberts HC, Rowley HA. Quantification and reproducibility of tracking cortical extent of activation by use of functional MR imaging and magnetoencephalography. Am J Neuroradiol 2000;21:1377–1387. [PubMed: 11003268]

Schaefer M, Muhlnickel W, Grusser SM, Flor H. Reproducibility and stability of neuroelectric source imaging in primary somatosensory cortex. Brain Topogr 2002;14:179–189. [PubMed: 12002348]

Sereno MI, Dale AM, Reppas JB, Kwong KK, Belliveau JW, Brady TJ, Rosen BR, Tootell RBH. Borders of multiple visual areas in humans revealed by functional resonance magnetic imaging. Science 1995;268:889–893. [PubMed: 7754376]

Shattuck DW, Leahy RM. BrainSuite: An automated cortical surface identification tool. Med Image Anal 2002;6:129–142. [PubMed: 12045000]

Stippich C, Freitag P, Kassubek J, Saras P, Kamada K, Kober H, Scheffler K, Hopfengartner R, Bilecen D, Radu EW, Vieth JB. Motor, somatosensory and auditory cortex localization by fMRI and MEG. Neuroreport 1998;9:1953–1957. [PubMed: 9674573]

Strupp JP. Stimulate: A GUI based fMRI analysis software package. Neuroimage 1996;3:S607.

Talavage TM, Sereno MI, Melcher JR, Ledden PJ, Rosen BR, Dale AM. Tonotopic organization in human auditory cortex revealed by progressions of frequency sensitivity. J Neurophysiol 2004;91:1282–1296. [PubMed: 14614108]

Vanni S, Warnking J, Dojat M, Delon-Martin C, Bullier J, Segebarth C. Sequence of pattern onset responses in the human visual areas: an fMRI constrained VEP source analysis. Neuroimage 2004;21:801–817. [PubMed: 15006647]

Vanni S, Dojat M, Warnking J, Delon-Martin C, Segebarth C, Bullier J. Timing of interactions across the visual field in the human cortex. Neuroimage 2004;21:818–828. [PubMed: 15006648]

Vitacco D, Brandeis D, Pascual-Marqui R, Martin E. Correspondence of Event-Related Potential Tomography and Functional Magnetic Resonance Imaging During Language Processing. Hum Brain Mapp 2002;17:4–12. [PubMed: 12203683]

Warnking J, Dojat M, Guerin-Dugue A, Delon-Martin C, Olympieff S, Richard N, Chehikian A, Segebarth C. FMRI retinotopic mapping-step by step. Neuroimage 2002;17:1665–1683. [PubMed: 12498741]

Wolters CH, Anwander A, Tricoche X, Weinstein D, Koch MA, MacLeod RS. Influence of tissue conductivity anisotropy on EEG/MEG field and return current computation in a realistic head model: A simulation and visualization study using high-resolution finite element modeling. Neuroimage. 2006in press

Yao J, Dewald PA. Evaluation of different cortical source localization methods using simulated and experimental EEG data. Neuroimage 2005;25:369–382. [PubMed: 15784415]

Zhang X, van Drongelen W, Hecox K, Towle VL, Frim DM, McGee A, He B. High Resolution EEG: Cortical Potential Imaging of Interictal Spikes. Clin Neurophysiol 2003;114:1963–1973. [PubMed: 14499758]

Zhang YC, Ding L, van Drongelen W, Hecox K, Frim D, He B. Cortical potential imaging by means of the finite element method and its application to simultaneous extra- and intra-cranial electrical recordings. NeuroImage 2006;31(4):1513–1524. [PubMed: 16631381]

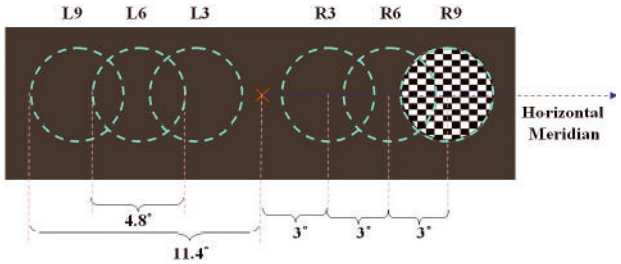

Figure 1.
Stimuli used in the present experiments. Circular checkerboards were flashed one at time at six different locations. The dashed circles represent the locations of the checkerboards.

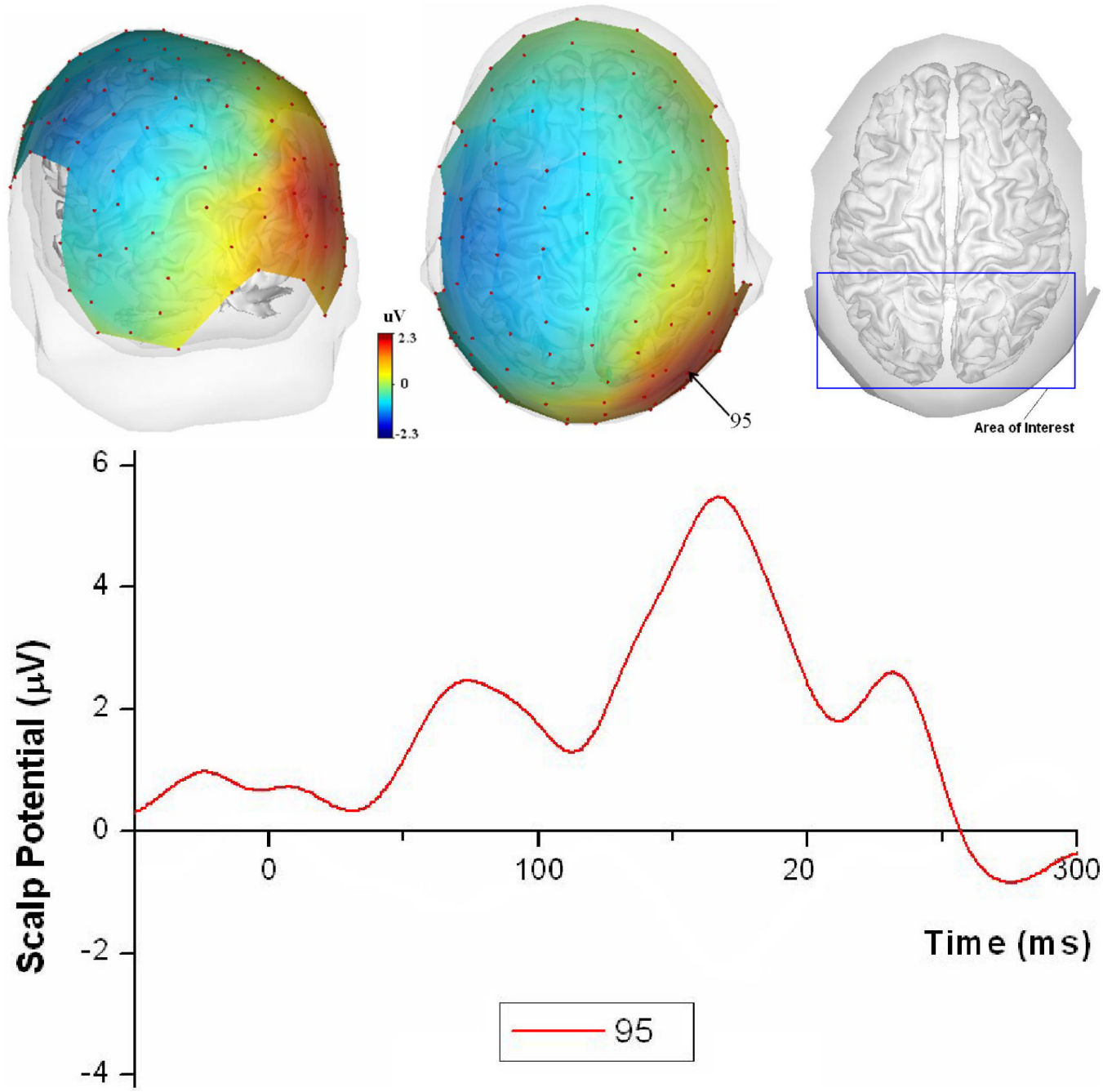

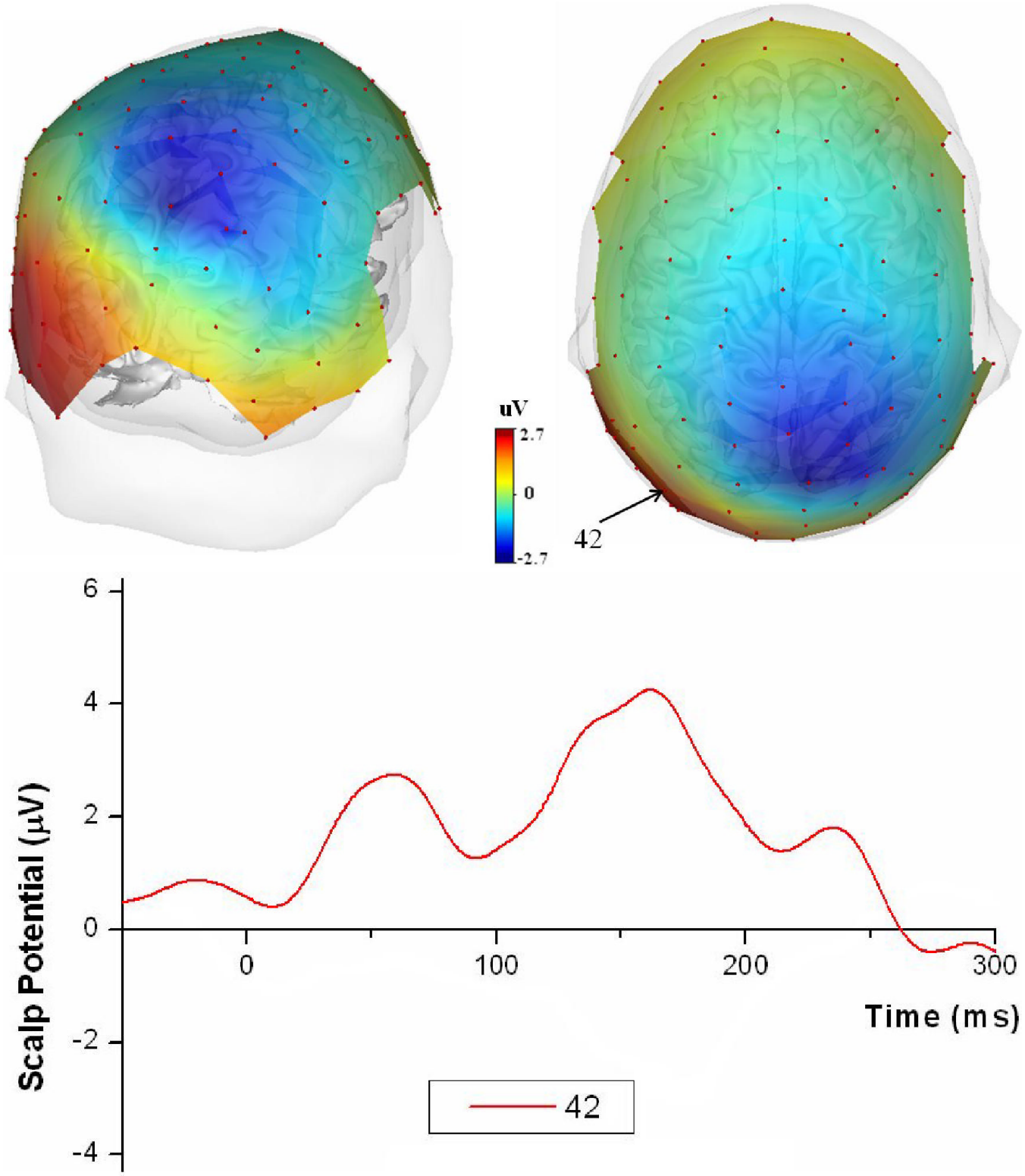

Figure 2.
Examples of topographic maps of the earliest VEP component and typical waveforms (subject 1): (a) a topographic potential map for protocol L9 (t = 73 ms) and the area of interest; (b)

waveforms at electrode 95, which is marked in (a); (c) a topographic map for protocol R3 (t = 59 ms); (d) waveforms at electrode 42, which is marked in (c). Tessellated cortical surface and boundary element model were visualized together with the topographic maps.

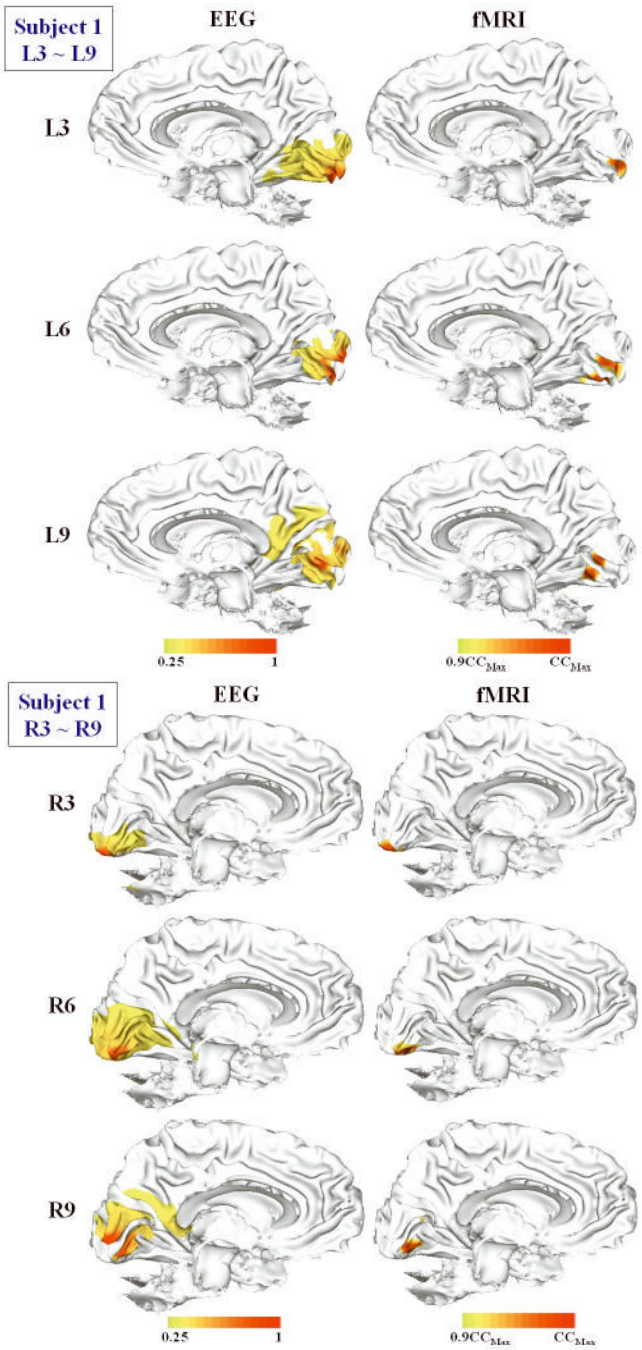

Figure 3.
Comparison of EEG cortical sources and fMRI activation maps for subject 1 (median sagittal view): (a) left stimuli; (b) right stimuli. The variables used in EEG cortical source images are normalized source power. For the fMRI maps, activations which exceeded 0.9 × maximum CC were visualized. For EEG maps, normalized source power below 0.25 was cut out from the visualization.

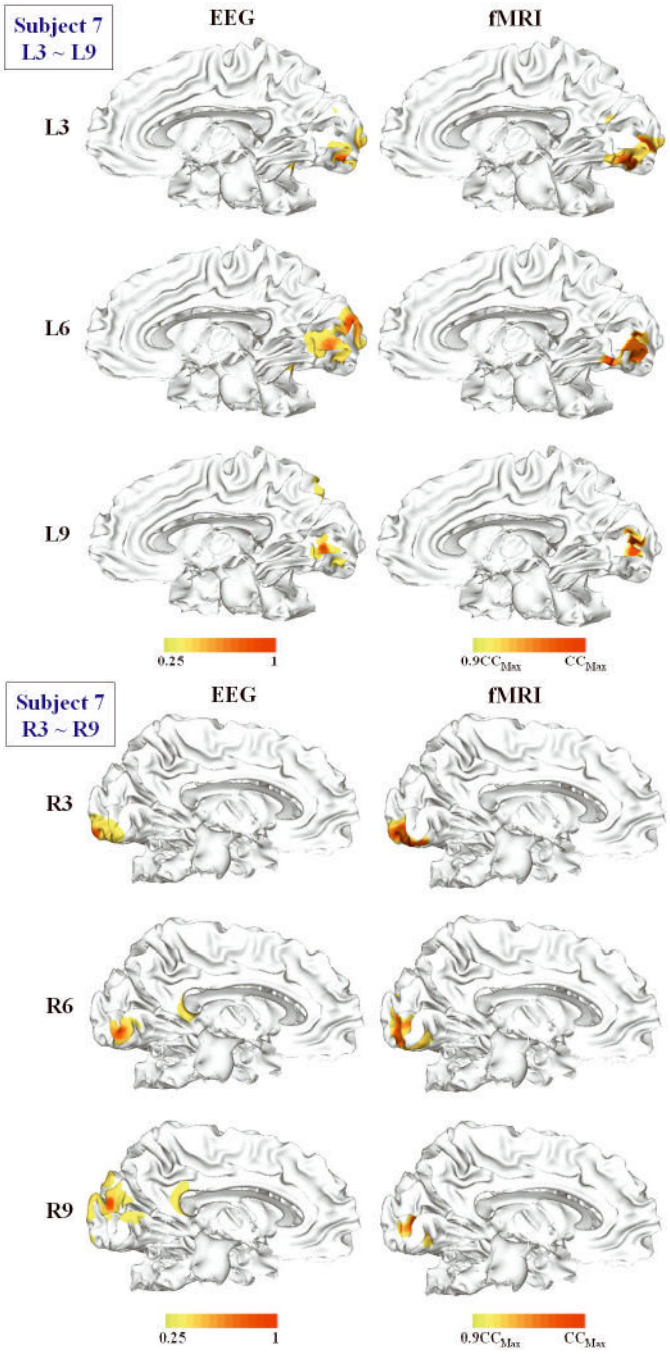

Figure 4.
Comparison of EEG cortical sources and fMRI activation maps for subject 7 (median sagittal view): (a) left stimuli; (b) right stimuli. The visualization conditions were the same as in Figure 3.

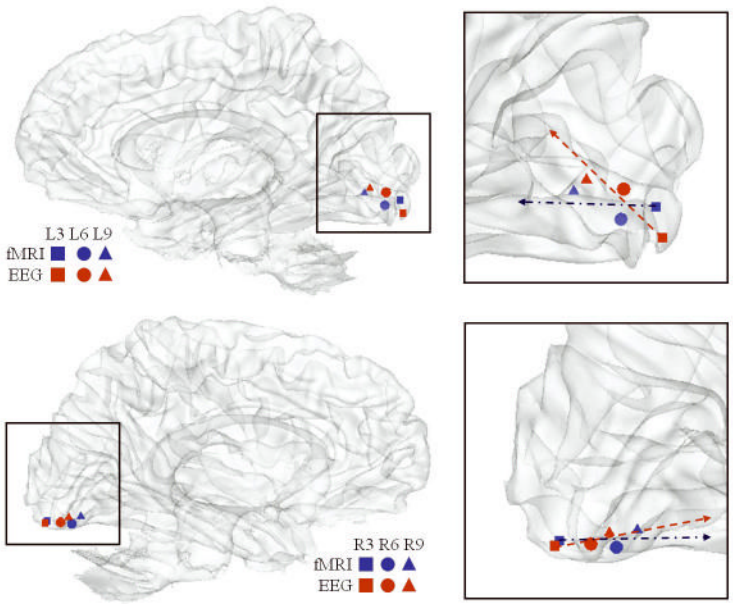

Figure 5.

Locations of fMRI and EEG sources coregistered in a single cortical surface model (subject 1). Right figures show the enlarged images around the primary visual cortex. Blue and red colors represent fMRI centers and EEG source peaks, respectively. Rectangular, circular, and triangular markers represent 3°, 6°, and 9° visual field changes, respectively. Red dashed line and blue dash-dot line represent first-order approximations of moving direction from the starting point (rectangular marker) in fMRI and EEG results, respectively. The angles between fMRI and EEG moving directions were 28.9° (left stimuli) and 7.8° (right stimuli).

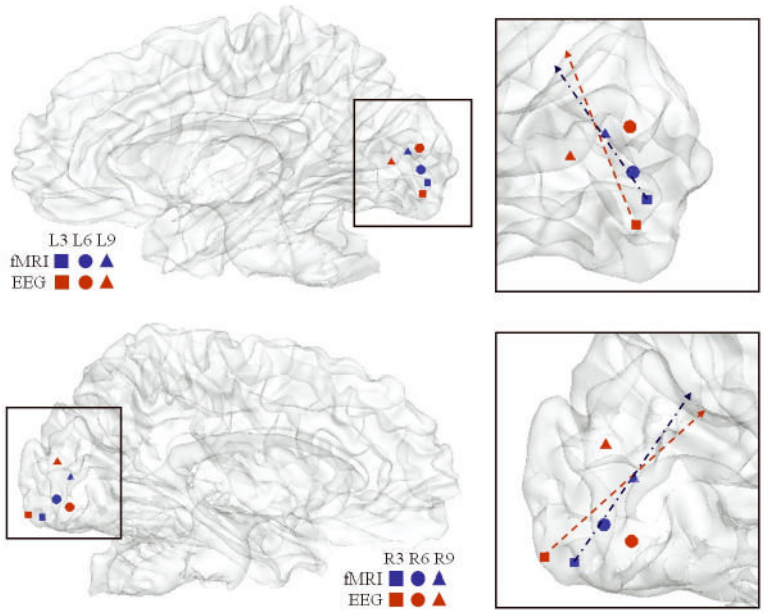

Figure 6.
Locations of fMRI and EEG sources coregistered in a single cortical model (subject 7). Descriptions are the same as in Figure 5. The angles between fMRI and EEG moving directions were 7.7° (left stimuli) and 12.0° (right stimuli).

TABLE I

Location error between fMRI centers and EEG source peaks. Average moving distances of fMRI centers and EEG peaks with respect to 3° and 6° visual field changes are also presented for comparison.

Subject #	Mean Location error (mm)	Average moving distance of fMRI centers with respect to 3° visual field change (mm)	Average moving distance of fMRI centers with respect to 6° visual field change (mm)	Average moving distance of EEG peaks with respect to 3° visual field change (mm)	Average moving distance of EEG peaks with respect to 6° visual field change (mm)
1	5.2	9.6	16.1	8.6	16.3
2	6.6	5.2	8.1	7.2	11.6
3	7.0	5.5	10.0	9.6	13.7
4	8.6	5.5	9.3	9.1	13.4
5	6.4	7.8	15.4	9.9	9.8
6	8.5	9.2	12.9	9.8	19.1
7	8.1	11.4	17.4	17.9	22.5
Median	7	7.8	12.9	9.6	13.7
25%, 75%	6.45	5.5	9.475	8.725	12.05
percentiles	8.4	9.5	15.925	9.875	18.4

TABLE II

Angles between two vectors each connecting first (3° visual field) and second (6° visual field) activations and second (6° visual field) and third (9° visual field) activations.

Subject #	Type of Stimuli	Bending angles (moving direction change) – fMRI (°)	Bending angles (moving direction change) – EEG (°)
1	Left	50.7	37.1
	Right	46.2	27.7
2	Left	63.4	59.8
	Right	32.5	41.6
3	Left	55.9	68.3
	Right	36.8	80.3
4	Left	6.4	36.5
	Right	9.5	35.6
5	Left	12.0	55.8
	Right	7.1	27.6
6	Left	78.6	81.1
	Right	77.4	11.2
7	Left	7.4	66.6
	Right	1.2	89.1
Median (25%, 75% percentile)	Left	50.7 (8.55, 61.53)	59.8 (41.78, 67.88)
	Right	32.5 (7.7, 43.85)	35.6 (27.63, 70.63)

TABLE III

Difference of mean moving directions between fMRI and EEG activations.

Subject #	Type of Stimuli	Angle between mean moving directions of fMRI and EEG activations (°)
1	Left	22.3
	Right	7.5
2	Left	29.7
	Right	13.7
3	Left	28.9
	Right	7.8
4	Left	10.0
	Right	6.8
5	Left	20.0
	Right	19.5
6	Left	1.2
	Right	10.1
7	Left	7.7
	Right	12.0
Median (25%, 75% percentile)	Left	20 (8.28, 27.25)
	Right	10.1 (7.58, 13.28)